Temperature-dependent CO2 line mixing models using dual frequency comb absorption and phase spectroscopy up to 25 bar and 1000 K

Ryan Cole, Ha Tran, Nazanin Hoghooghi, Gregory Rieker

Temperature-dependent CO_2 Line Mixing Models using Dual Frequency Comb Absorption and Phase Spectroscopy up to 25 bar and 1000 K

Ryan K. Cole[1], Ha Tran[2], Nazanin Hoghooghi[1], Gregory B. Rieker[1]

[1]*Precision Laser Diagnostics Laboratory, Department of Mechanical Engineering, University of Colorado Boulder 1111 Engineering Drive, Boulder CO, USA 80309*

[2]*Laboratoire de Météorologie Dynamique, IPSL, CNRS, Sorbonne Université, Ecole Polytechnique, Institut Polytechnique de Paris, Ecole normale Supérieure, PSL Research University, Paris F-75005, France*

Abstract

We perform dual frequency comb laser absorption spectroscopy of CO_2 at high pressure and temperature, and use the spectra to test and improve CO_2 line mixing models and their temperature dependence. The dual-comb spectrometer spans 6800-7000 cm^{-1} with 0.0066 cm^{-1} point spacing, and is coupled to a specialized, high-pressure, high-temperature gas cell providing conditions up to 977 K and 25 bar. We compare our measurements to spectra calculated using an advanced line mixing model for pure CO_2 based on the energy-corrected sudden (ECS) approximation. We determine a new set of temperature-dependent ECS model parameters, and show that the new parameters significantly improve the accuracy of the ECS line mixing model over a temperature range spanning 298-977 K. We also compare the measured spectra to a simpler line mixing model developed using the modified exponential gap (MEG) scaling law, and report the temperature and pressure dependence of the MEG model parameters required to scale the model across wide ranges of conditions. Finally, we report high-pressure, ambient-temperature measurements of CO_2 spectra in both amplitude (absorption) and phase using the dual-comb spectrometer. We use these measured absorption and phase spectra to assess the performance of the ECS and MEG line mixing models at high densities near room temperature. To the best of our knowledge, these results represent the first study of line mixing using phase spectroscopy. Overall, the results of this study significantly expand line mixing models for CO_2 at high pressure and temperature and improve the accuracy and availability of absorption models for harsh conditions encountered in laser-based sensing and planetary science.

1. Introduction:

Accurate models for absorption spectra at high pressure and temperature are required as inputs to radiative transfer models for exotic planetary atmospheres and to support laser-based sensors for combustion, propulsion, and energy conversion systems [1–4]. Absorption spectroscopy of CO_2 is particularly important in these applications as CO_2 is a primary combustion byproduct as well as a significant, radiatively active component of many planetary atmospheres (e.g. Venus, ~96% CO_2, 93 bar, 730 K [5]). This paper seeks to improve the accuracy of absorption

models for CO_2 at high pressure and temperature using new laboratory spectra measured with a dual frequency comb absorption spectrometer in conditions up to 977 K and 25 bar.

Accurate absorption models for high-pressure, high-temperature conditions require both accurate databases of parameters to describe individual absorption transitions (e.g. intensities, center frequencies, broadening and pressure shift coefficients and their temperature dependence) as well as models for additional collisional phenomena (e.g. line mixing and finite collision durations) that become more significant at elevated pressures. Line mixing in particular has been shown to significantly affect the shape of measured spectra at elevated pressures [6,7]. Line mixing occurs as a result of collision-induced transfer of rotational population between the energy levels of the absorbing molecules, which in turn affects an exchange of absorption intensity between individual rovibrational transitions [6,7]. While there are many factors that ultimately govern its strength (see Ref. [6]), line mixing is significant in conditions when the line width of absorption transitions approaches or exceeds their frequency separation [6,7]. Such conditions include high pressure gases or spectral regions with densely spaced lines (e.g. band heads or Q branches) [6]. Under these conditions, the omission of line mixing in absorption models has been shown to cause significant deviations between measured and modeled spectra.

Line mixing in CO_2 has received considerable experimental and theoretical interest throughout the last several decades [8–24]. While these past studies have considered a range of CO_2 bands throughout the near- and mid-infrared, our present study focuses specifically on line mixing in the near infrared CO_2 bands between 6800 and 7000 cm^{-1}. CO_2 absorption in this region is dominated by the $3\nu_3$ band (00031←00001) and a number of adjacent hot bands. Most past investigations of line mixing in these bands target high pressure conditions near room temperature [9,11–15,17,22,23,25,26]. To the best of our knowledge, only two prior studies have investigated line mixing in these bands at elevated temperature *and* pressure conditions (40+ bar and 473 K) [11,17].

The present study is focused on improving line mixing models and their temperature dependence for the case of pure CO_2. Tran et al. [11] developed an advanced line mixing model for pure CO_2 using the energy-corrected sudden (ECS) approximation [27]. This approximation (discussed in more detail in Section 3) is generally regarded as a physically realistic approach to model line mixing because it permits the calculation of the state-to-state collisional transfer rates while also properly accounting for the coupling of angular momenta in the collision process [6,8,

28,29]. Tran *et al.* showed that the pure CO_2 ECS model accurately reproduces the shape of many CO_2 bands (including bands in the 6800-7000 cm^{-1} region) across a range of temperatures up to 473 K and for pressures in excess of 40 bar [11].

A remaining challenge in the development of CO_2 line mixing models lies in extending the models to high-temperature conditions relevant to combustion and planetary science. While there are some notable exceptions (e.g. [10,11,17,19,30–36]), the vast majority of the past experimental and theoretical line mixing studies have considered only lower temperature conditions, presumably due to the experimental challenges associated with measuring accurate, high-pressure, high-temperature reference spectra needed to develop and validate absorption models for these conditions. A consequence is that existing models must be significantly extrapolated in order to calculate spectra for high temperature applications in combustion and planetary science.

In this paper, we use new measurements of pure CO_2 spectra in conditions up to 977 K and 25 bar to evaluate and improve models for CO_2 line mixing and its temperature dependence. Our study reports measurements from a broadband, high-resolution dual frequency comb spectrometer coupled with a specialized, high-pressure, high-temperature gas cell [37]. We use this unique experimental configuration to record spectra of pure CO_2 between 6800 and 7000 cm^{-1} with a point spacing of 0.0066 cm^{-1} over a matrix of pressure and temperature conditions up to 25 bar and 977 K. Using these measurements, we report three primary results:

- We update and validate the pure-CO_2 line mixing model of Tran et al. [11] over an expanded range of temperatures and pressures up to 977 K and 25 bar, and we use our high-temperature measurements to parameterize the temperature dependence of the ECS model parameters required to scale the model across wide temperature ranges.
- We compare our measurements and the updated ECS model to a simpler model developed using a modified exponential gap (MEG) scaling law, and we report new values for the temperature- and pressure-dependence of the MEG model parameters.
- We explore (for the first time) the use of phase spectra for fundamental studies of line mixing at elevated pressures.

Taken as a whole, these results significantly expand line mixing models for pure CO_2 at high pressure and temperature and improve the accuracy of absorption models for applications in laser-based sensing and planetary science.

2. Experiment and Data Collection:

The spectra for this study were measured in the specialized, high-pressure, high-temperature gas cell described in detail in Ref. [37]. Briefly, the gas cell consists of a ceramic tube furnace housed inside of a custom pressure vessel. The absorbing gas (CO_2 in this case) is confined at the center of the ceramic furnace in a $45.82^{+0.11}_{-0.34}$ cm quartz sample cell. The quartz cell is surrounded in the tube furnace by a molybdenum cylinder that acts as a heat spreader to increase the temperature uniformity of the sample gas. The outer pressure vessel is filled with a non-absorbing bath gas (argon in this study), which is carefully controlled to ensure that a slight positive pressure differential is maintained relative to the quartz sample cell. In this configuration, the quartz cell experiences only a slight pressure differential and does not rupture regardless of the absolute pressures in the gas cell. Light from the spectrometer is passed axially through the gas cell to record the spectrum of the absorbing gas at the conditions of the sample cell. This configuration is shown schematically in Figure 1.

The temperature distribution of the sample cell is monitored by seven K-type thermocouples (including two immersed in the sample gas within the sample cell). The temperature uniformity (defined as the maximum percent deviation from the mean temperature) is better than 5% for all conditions reported in this paper. Due to the wide range of pressures

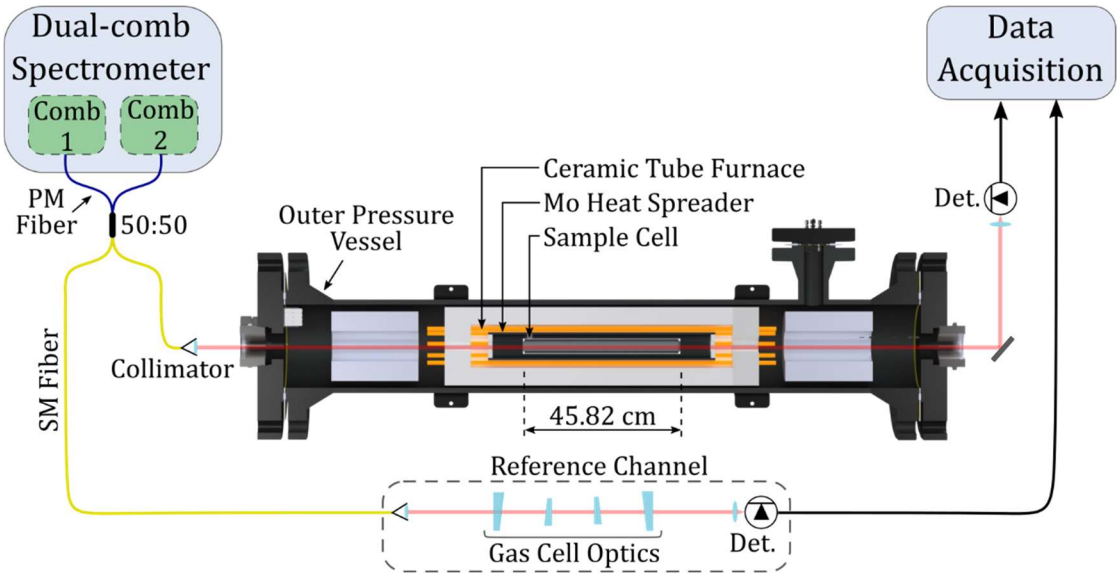

Figure 1: Simplified schematic of the high-pressure, high-temperature gas cell along with the configuration of the dual-comb spectrometer used in this study.

Temperature (K)	Pressure (bar)	Density (amg)
495±7	1.99±0.01	1.08±0.02
495±7	4.97±0.02	2.70±0.04
495±7	9.30±0.05	5.07±0.07
493±7	25.0±0.1	13.8±0.02
735±10	2.01±0.01	0.73±0.01
733±10	4.98±0.02	1.82±0.03
731±10	10.06±0.05	3.68±0.05
730±10	20.0±0.1	7.4±0.1
977±13	1.99±0.01	0.546±0.008
972±13	4.96±0.02	1.37±0.02
967±13	10.05±0.05	2.78±0.04
964±13	14.9±0.1	4.13±0.06

Table 1: List of the experimental temperatures (K), pressures (atm), and densities (amagat) of the spectra reported in this study.

measured in this study, the sample gas pressure is monitored by three calibrated capacitance manometers optimized for different pressure ranges. The first is optimized for pressures below 1.3 bar (MKS Baratron 626C, accuracy 0.25% of reading), the second is optimized for 1.3-13 bar (MKS Baratron 121A, accuracy 0.5% of reading), and the third is optimized for higher pressures (MKS Baratron 750C, accuracy ±0.1 bar).

We combine the high-temperature, high-pressure gas cell with a broadband, high-resolution, fiber mode-locked dual frequency comb spectrometer (DCS) [38]. The specific dual-comb spectrometer used in this work consists of two self-referenced erbium fiber mode-locked frequency combs with a nominal comb tooth spacing of ~0.0066 cm^{-1} [39–42]. The optical bandwidth of the two combs spans ~5500-8000 cm^{-1}, which we filter for this study to cover ~6800-7000 cm^{-1}. The pulse repetition rate of each frequency comb (which determines the comb tooth spacing) is stabilized to a common CW reference laser (RIO ORION) that operates at 1565 nm with a linewidth <5 kHz. A simple feedback to the reference laser frequency stabilizes the ~200 MHz repetition rate of each frequency comb to within ±5 Hz. All measurements of the lock frequencies and repetition rates are referenced to a GPS-disciplined oscillator (Jackson Labs Fury) with stability better than 10^{-11}. We conservatively estimate the absolute accuracy of the DCS system to be ~1.7×10^{-4} cm^{-1}, which is limited by the stabilization of the reference laser.

Using the experimental configuration described above, we record spectra of $^{12}C^{16}O_2$ (Airgas Instrument Grade, >99.99% purity) at the twelve temperature and pressure conditions listed in Table 1. In Table 1, we also report the density (in amagat, amg), which is computed from the experimental temperature and pressure using the NIST-recommended equation of state for CO_2 [43,44]. The uncertainty in the reported gas temperature is a combination of the standard uncertainty for a K-type thermocouple (0.75% of reading) and the uncertainty associated with a radiation correction applied to our temperature measurements (see Ref. [37]). The uncertainties in the measured pressures are based on the reported accuracy of the capacitance manometers used to monitor the pressure in the sample gas cell (discussed above). Uncertainty in the gas density is determined based on the corresponding uncertainty in temperature and pressure.

We record spectra for 30 to 90 minutes and use a coherent averaging technique to increase the signal to noise ratio [45]. To account for the non-absorbing intensity spectrum of the DCS (the "baseline"), we normalize each measured spectrum using a vacuum background spectrum taken through the sample cell prior to the experiment as well as a second spectrum recorded simultaneous to the experiment through an optical path that passes though the same optics as the gas cell (quartz and sapphire windows) but does not pass though the gas cell itself. In practice, some degree of residual baseline variation remains after this normalization process. We remove the remaining baseline variation using a Chebyshev polynomial fit to the measured spectra. We discuss the baseline correction process developed for this study and its associated uncertainty in more detail in the Appendix. In the Appendix, we also assess the integrated intensities of the measured spectra (as a test of the quality of the baseline-corrected spectra), and show that the integrated intensities agree with their predicted values based on the HITRAN2020 database within ~2% [46].

Lastly, although all portions of the optical path are continuously purged with dry air, some residual water vapor absorption is present in the measured spectra. This interfering absorption is due to water vapor in the argon bath gas surrounding the quartz sample cell. We fit and subtract the background absorption using a speed-dependent Voigt profile and high-temperature line shape parameters for argon-broadened water vapor [47].

3. Line Mixing Model

3.1. General Equations

To model line mixing in our measured spectra, we follow the relaxation matrix formalism commonly employed in the literature. Detailed summaries of this approach are given in Refs. [6,7] and references therein. Here we only list the salient details. Under the impact approximation, the absorption coefficient at wavenumber ν is given by [6,7]

$$\alpha(\nu) = N\frac{8\pi^2\nu}{3hc}\left[1 - e^{-\frac{hc\nu}{k_bT}}\right]\sum_{\ell}\sum_{\mathscr{k}}\rho_\ell(T)d_\ell d_{\mathscr{k}}Im\left\{\langle\langle\mathscr{k}\left\|[\boldsymbol{\Sigma} - \boldsymbol{L_o} - iN\boldsymbol{W}(T)]^{-1}\right\|\ell\rangle\rangle\right\} \quad (1)$$

where the sums include all lines of the absorbing gas with indices ℓ and $\mathscr{k}$. N is the number density of the absorbing gas, ρ is the lower-state Boltzmann population fraction, and d is the dipole matrix element. Bolded terms correspond to matrices, and $\langle\langle\mathscr{k}\|\cdot\|\ell\rangle\rangle$ indicates a matrix element. $\langle\langle\mathscr{k}\|\boldsymbol{\Sigma}\|\ell\rangle\rangle = \nu \times \delta_{\ell\mathscr{k}}$ corresponds to the frequency of the calculation, $\langle\langle\mathscr{k}\|\boldsymbol{L_o}\|\ell\rangle\rangle = \nu_\ell \times \delta_{\ell\mathscr{k}}$ corresponds to the resonant frequency of each transition ℓ, and $\boldsymbol{W}(T)$ is the collisional relaxation matrix. The absorption coefficient calculated using Equation 1 neglects Doppler broadening effects as well as the influence of speed dependence and velocity-changing collisions.

The complex collisional relaxation matrix contains all of the collisional information for the absorbing molecule. The diagonal elements correspond to the pressure broadening (γ) and shift (δ) coefficients for each transition [6,7]

$$\langle\langle\ell\|\boldsymbol{W}(T)\|\ell\rangle\rangle = \gamma_\ell(T) - i\delta_\ell(T) \quad (2)$$

The off-diagonal components give a measure of the coupling between individual transitions, such that $\langle\langle\mathscr{k}\|\boldsymbol{W}(T)\|\ell\rangle\rangle$ corresponds to the rate of collisional transfer from the states associated with line ℓ into the states associated with line $\mathscr{k}$. The relaxation matrix also satisfies two fundamental relations known as detailed balance and the sum rule. The detailed balance principle relates the transpose elements as

$$\langle\langle\mathscr{k}\|\boldsymbol{W}(T)\|\ell\rangle\rangle \times \rho_\ell(T) = \langle\langle\ell\|\boldsymbol{W}(T)\|\mathscr{k}\rangle\rangle \times \rho_{\mathscr{k}}(T) \quad (3)$$

and the sum rule states that

$$\sum_{\mathscr{k}} d_{\mathscr{k}}\langle\langle\mathscr{k}\|\boldsymbol{W}(T)\|\ell\rangle\rangle = 0 \quad (4)$$

or equivalently

$$\sum_{\mathscr{k}\neq\ell}\frac{d_{\mathscr{k}}}{d_\ell}\langle\langle\mathscr{k}\|\boldsymbol{W}(T)\|\ell\rangle\rangle = -\gamma_\ell \quad (5)$$

As mentioned above, the off-diagonal elements of $\boldsymbol{W}$ correspond to the couplings between individual transitions in the absorption spectrum. As such, these elements are the critical quantities that must be calculated in order to model the absorption spectrum using Equation 1. We will discuss methods used to calculate the off-diagonal components of the relaxation matrix in the remainder of this section.

3.2. Energy Corrected Sudden Scaling Law

Many past studies have modeled the relaxation matrix for CO_2 using the energy corrected sudden (ECS) scaling law [9,11,18,28,29,48]. The physical basis of this scaling law has been described in detail in Refs. [6,7] (and references therein). For the purpose of this paper, we summarize that the ECS scaling law enables calculation of collisional population transfer rates while also properly accounting for angular momentum transfer during collisions [6,28,29]. Here, we follow the specific form of the ECS scaling law that has been used in previous studies to model line mixing in the CO_2-air and pure CO_2 systems [11,18,28,29]. Under the ECS scaling law, the real component of the relaxation matrix is expressed as [11,18,28,29]

$$Re\langle\langle \mathscr{k} \| \boldsymbol{W}(T) \| \ell \rangle\rangle = (-1)^{l_{2i}+l_{2f}}(2j_i'+1)\sqrt{(2j_f'+1)(2j_f+1)} \times$$
$$\sum_{L_{even}\neq 0} \begin{pmatrix} j_i & L & j_i' \\ l_{2i} & 0 & -l_{2i} \end{pmatrix} \begin{pmatrix} j_f & L & j_f' \\ -l_{2f} & 0 & l_{2f} \end{pmatrix} \begin{Bmatrix} j_i & j_f & 1 \\ j_f' & j_f & L \end{Bmatrix} (2L+1)\frac{\Omega(j_i,T)}{\Omega(L,T)} Q(L,T) \qquad (6)$$

where j_i and j_f are the initial and final rotational quantum numbers for transition ℓ, j_i' and j_f' are the rotational quantum numbers corresponding to transition $\mathscr{k}$, and l_2 is the vibrational angular momentum quantum number. $(\because)$ and $\{\because\}$ denote Wigner 3J and 6J coefficients [49], respectively.

In Equation 6, Ω is an adiabaticity correction that accounts for molecular rotation during collisions [11,18,28,29]

$$\Omega(j,T) = \left(1 + \frac{1}{24}\left(\frac{\omega_{j,j-2}d_c}{\bar{v}(T)}\right)^2\right)^{-2} \qquad (7)$$

where d_c is a scaling length, and $\bar{v}(T)$ is the mean relative speed. $\omega_{j,j-2}$ is the frequency spacing between the j and $j-2$ rotational levels. The rotational cross sections $Q(L,T)$ are given by

$$Q(L,T) = A(T)[L(L+1)]^{-\lambda(T)}e^{-\beta\frac{hcE_L}{k_bT}} \qquad (8)$$

where E_L is the rotational energy of level L [11,18,28,29]. In Equations 6-8, $d_c, A(T), \lambda(T)$ and β are the free parameters of the ECS model that can be deduced from experimental data (described in more detail below).

3.3. Modified Exponential Gap Scaling Law

A second method to model the relaxation matrix is based on simpler energy-gap scaling laws [6,7]. As the name suggests, these scaling laws parameterize collisional population transfer according to the energy difference between the involved states. This approach has been used to model line mixing in CO_2 in a number of previous studies [10,19,24,35,36,50]. Using the energy-gap approach, the real part of the off-diagonal relaxation matrix elements are proportional to the thermally averaged collisional population transfer rates (K), such that [6,7]

$$Re\langle\langle \mathscr{k} \| \boldsymbol{W}(T) \| \ell \rangle\rangle \propto K_{j_i j_i'} \tag{9}$$

where j_i and j_i' are the lower levels of transitions ℓ and $\mathscr{k}$, respectively. Equation 9 is an equality only in the case of isotropic Raman Q-branches [6], and we will discuss the relationship between the population transfer rates and the relaxation matrix for multibranch infrared spectra in more detail in Section 4.2.

There are many forms of energy-gap scaling laws (see Ref. [6,7,51]), however here we will consider the modified exponential gap (MEG) scaling law. Under the MEG law, the collisional transfer rates are given by [6,7]

$$K_{j_i j_i'} = a_1(T) \left[\frac{1 + 1.5\left(\frac{E_{j_i}}{a_2 k_b T}\right)}{1 + 1.5\left(\frac{E_{j_i}}{k_b T}\right)} \right]^2 \exp\left(-\frac{a_3 \Delta E}{k_b T}\right) \tag{10}$$

where E_{j_i} is the energy of state j_i (equivalently, the lower state energy of transition ℓ) and ΔE is the energy difference between states j_i and j_i'. a_i are the free parameters of the model that are deduced from experimental data.

The MEG model differs from the ECS model (Equation 6) in several important ways. It is considerably simpler to implement, which has promoted adoption in applied settings [33–36] or in cases where more advanced models are not available. However, the MEG model requires significant *ad hoc* modifications to address effects such as mixing between lines in different branches (inter- vs. intra-branch mixing) as well as mixing between levels with different parities [6,7]. These effects are governed by angular momentum transfer, and not the energy gap between

the involved states. As such, these effects are automatically rectified by the ECS model, which is widely considered to be a much more physically realistic model for collisional population transfer.

4. Results and Discussion

4.1. Updated ECS Model for Temperatures up to 977 K

As mentioned above, Tran et al. [11] have previously developed an advanced line mixing model for pure CO_2 using the ECS scaling law. This model was validated against high-pressure spectra measured at temperatures up to 473 K. The high-temperature spectra measured in the present study give us the opportunity to test the model against spectra measured at temperatures up to 977 K, and to parameterize the temperature dependence of the model parameters so that the model can be scaled across wide temperature ranges.

To implement the ECS model, we first determine the free parameters of the model through fits to measured broadening coefficients, which are related to the real part of the relaxation matrix via the sum rule. In this process, we employ our previous low-pressure study of CO_2 in this wavenumber range (6800-7000 cm^{-1}) that reports broadening coefficients for transitions in the $3\nu_3$ band at four temperatures between 296 K and 980 K [52]. To determine the best fit parameters, we compare these measured broadening coefficients to the broadening coefficients calculated using the sum rule (Equations 4-5) and the ECS scaling law. To account for the temperature dependence of the model parameters, we parametrize the temperature-dependent parameters A and λ using the power-law temperature scaling, which is widely used for the line broadening coefficient and adopted in past studies [29,48] for A and λ, i.e.:

$$A(T) = A(296)\left(\frac{296}{T}\right)^{n_A} \tag{11}$$

where $A(296)$ is determined at 296 K, and n_A scales the parameter to different temperatures T. We adopt an analogous equation for the parameter λ.

In practice, multiple sets of model parameters can yield sufficient fits to the measured broadening coefficients. As such, the best-fit parameter set is chosen as the set that both reasonably fits the measured broadening coefficients *and* leads to the best agreement between calculated spectra and the spectra measured for this study. Table 2 lists the best fit parameters for the updated ECS model. The updated model parameters lead to improved agreement with measured broadening

	d_c [Å]	$A(296)\left[\frac{cm^{-1}}{atm}\right]$	n_A	$\lambda(296)$	n_λ	β
This Work	4.9	0.0207	0.011	0.072	-0.31	0.052
Tran *et al.* 2011	5.5	0.019	-	0.61	-	0.052

Table 2: List of the best-fit parameters for the ECS model along with the original parameter set given in Tran *et al.* 2011 [9]

coefficients over the temperature range spanning 296-980 K owing to the significant changes in the parameter values (namely λ and its temperature dependence). However, the two parameter sets yield similar calculations near room temperature due to the renormalization procedure [28] applied to the relaxation matrix.

After determining the ECS model parameters, we use the scaling law relationships and detailed balance (Equations 3, 6-8) to calculate the real components of the off-diagonal elements of the relaxation matrix. The imaginary components of the off-diagonal elements do not significantly affect the shape of calculated spectra, and we fix these elements at zero. We populate the diagonal elements according to Equation 2. For this step, we again employ the database of temperature-dependent broadening and pressure shift coefficients developed for this wavenumber range in our prior study [52]. These pressure broadening and shift coefficients have been validated for temperatures up to 980 K. Similar to prior studies, we neglect line mixing between transitions belonging to different vibrational levels because collisional population transfer between these levels is expected to be extremely weak [6]. Finally, after constructing the relaxation matrix, we employ the renormalization procedure described in Ref. [28] to ensure that the relaxation matrix obeys detailed balance and the sum rule (Equations 3-5) exactly.

We calculate spectra according to Equation 1 using the relaxation matrix constructed with the ECS model. The calculation utilizes the relaxation matrices described above, as well as the absorption parameters (line centers, intensities, and lower state energies) listed in HITRAN2020 [46]. Figure 2 compares a spectrum measured at a temperature of 730 K and a pressure of 20.0 bar to spectra calculated using the updated ECS model, the original pure-CO_2 ECS model (Tran *et al.* 2011 [11]), and a Lorentzian model where line mixing is neglected.

Figure 2 shows that the updated ECS model parameters significantly improve agreement between the measured spectrum and the absorption model relative to both the original pure-CO_2

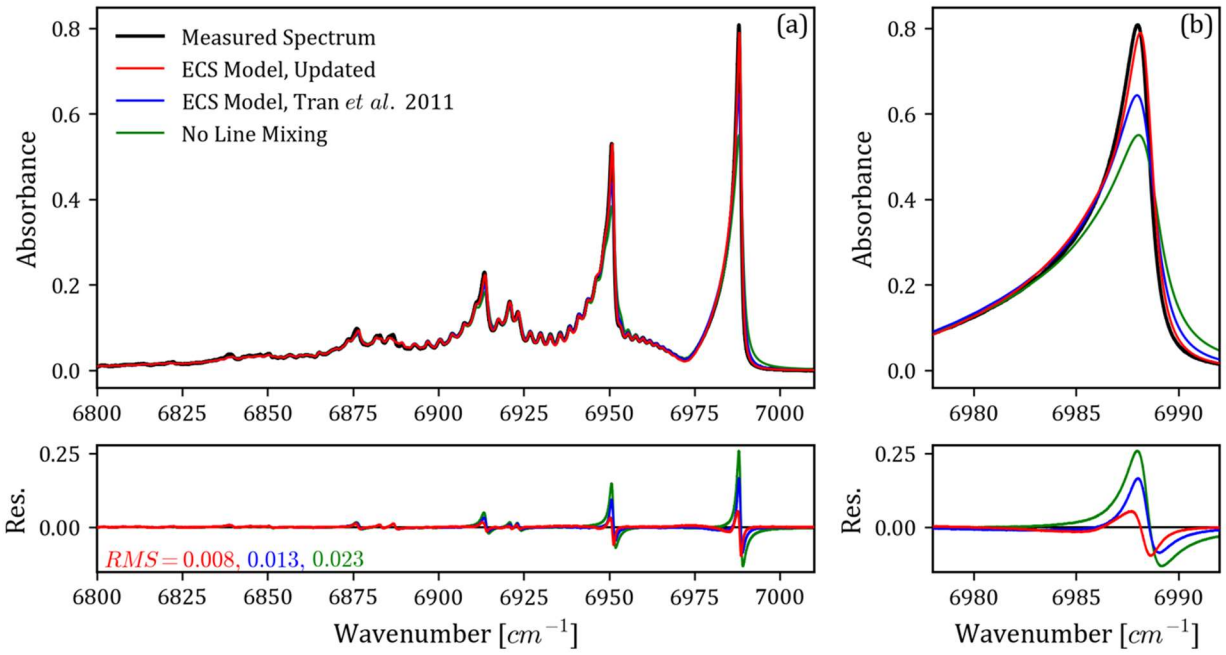

Figure 2: Comparison between the measured spectrum (black) and spectra calculated using the updated ECS model parameters (red), the parameters of Tran *et al.* 2011 (blue) and a Lorentzian model where line mixing is neglected (green). Measurement conditions are 730 K and 20.0 bar. Panel (a) shows the comparison for the full wavenumber range of the measurement, while panel (b) highlights the comparison for the $3\nu_3$ band head. The upper panels show the measured and calculated absorption spectra while their differences (Meas-Calc) are plotted in the lower panels. The updated ECS model parameters significantly improve agreement with the measured spectra

ECS model and the case where line mixing is neglected. The improvement due to the updated ECS model parameters is most dramatic in the band head regions where line mixing is strongest. Comparisons at other temperature and pressure conditions indicate that the new ECS parameters improve measurement-model agreement across the full range of conditions considered here (495-977 K, 2-25 bar).

Notably, we also compare the spectra calculated using the updated parameters to calculations using the original (Tran *et al.* 2011 [11]) parameters near room temperature. One such comparison is shown in Figure 3. This comparison shows that the two parameter sets yield comparable results near 296 K when compared to a spectrum calculated without line mixing effects. A direct comparison of the two ECS calculations shows that the model calculations differ by less than ~5% over a range of pressures up to ~25 bar. This fact indicates that the updated ECS model parameters retain the performance of the original ECS model near 296 K, while also significantly improving the accuracy of the model for high temperatures up to 977 K. We further

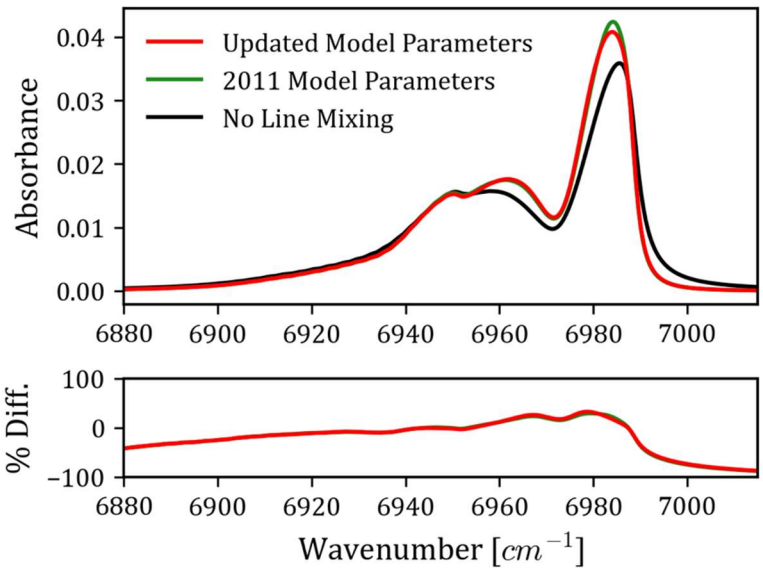

Figure 3: Comparison between a spectrum calculated using the ECS model parameters of Tran *et al.* 2011 [11] (green), a spectrum calculated using the updated ECS model parameters (red), and a spectrum calculated without line mixing effects (black). The spectrum is calculated at a temperature of 303 K and a pressure of 24.6 bar. The bottom panel shows the percent difference between the two ECS calculations and the model calculated neglecting line mixing effects.

assess the accuracy of the ECS model for high-pressure spectra measured near room temperature in Section 4.3.

4.2. MEG-ECS Comparisons

Similar to the ECS model, we determine the free parameters of the MEG model through fits to the broadening coefficients measured for transitions in the $3\nu_3$ band [52]. The MEG model assumes that only one of the parameters depends on temperature (a_1), and prior studies have shown that the temperature scaling of the a_1 parameter follows a single power law of the form [7,10,34]

$$a_1(T) = a_1(296)\left(\frac{296}{T}\right)^{n_{a_1}} \tag{11}$$

Here, we determine a_1 individually at each of the four temperatures corresponding to the measured broadening coefficients. The measured values agree well with Equation 11 with $n_{a_1} = 1.31$ over the full range of temperatures spanning 296-980 K. The measured MEG parameters are in reasonable agreement with the results of Hartmann *et al.* [10] who apply a similar form of the

MEG law to model line mixing in pure CO_2 [10]. Notably, our measured temperature dependence ($n_{a_1} = 1.31$) is in excellent agreement with Hartmann *et al.* [10], who also report $n = 1.31$ from high-temperature measurements of the v_3 band. Table 3 summarizes the best fit parameters for the MEG model.

As discussed in Section 3.3, when applied to infrared spectra, the MEG model only determines the real components of the off-diagonal relaxation matrix elements to within a constant of proportionality [6]. Here, we relate the relaxation matrix to the MEG-calculated transfer rates using an empirical parameter F that simultaneously scales the population transfer rates and accounts for mixing between transitions in different branches [6,50,53–58]. With this modification, the relaxation matrix is given by

$$Re\langle\langle \mathcal{k} \| \boldsymbol{W}(T) \| \mathcal{l} \rangle\rangle = \begin{cases} F \times K_{j_i j_i'} & \text{Intrabranch} \\ (1-F) \times K_{j_i j_i'} & \text{Interbranch} \end{cases} \quad (12)$$

where interbranch mixing denotes line mixing between lines in different branches (i.e. P↔R), and intrabranch indicates mixing between lines in the same branch (e.g. P↔P). Interbranch mixing is expected to be weaker than intrabranch mixing, but this effect depends on angular momentum transfer and is not properly accounted for in the MEG model (which considers only energy differences) [53,59–62].

Equation 12 cannot be directly applied to model three-branch spectra (P, Q, R). The strongest Q-branch transitions in the considered wavenumber range occur in the (01131←01101) hot band. These Q-branch transitions are three orders of magnitude weaker than the corresponding P- and R-branch transitions, and the peak Q-branch absorption is barely resolved above the noise level of our measurements. As such, we neglect interbranch line mixing between Q and R/P branches for the weak hot bands in our wavenumber range, which ultimately has little effect on the shape of calculated spectra. Finally, similar to the ECS calculations, our model neglects the

$a_1(296)\left[\frac{cm^{-1}}{atm}\right]$	n_{a_1}	a_2	a_3
0.0171	1.31	1.42	1.30

Table 3: Summarizes the best-fit parameters for the MEG model determined from fits to measured broadening coefficients [52].

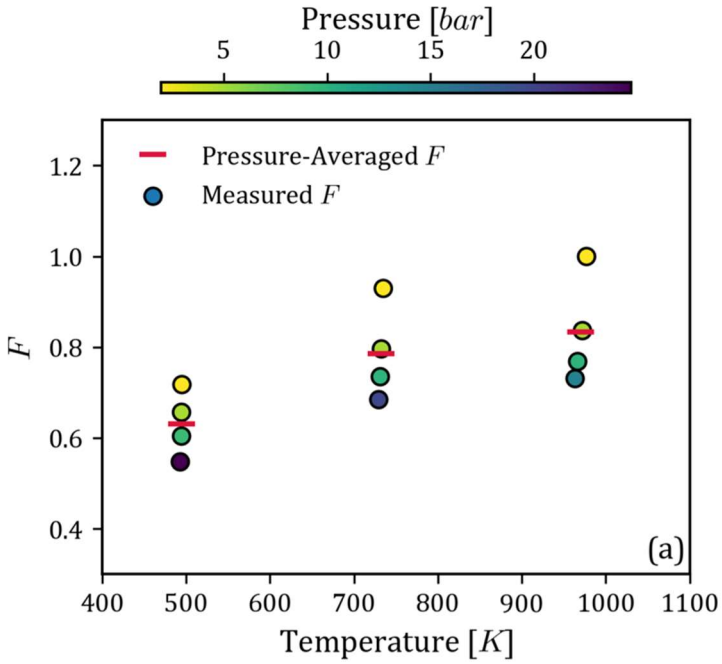

Figure 4: The measured values of the coefficient F that scales the relaxation matrix in the MEG model. The F values depend on both temperature and pressure. The pressure-averaged F value increases as gas temperature increases. At each temperature, F monotonically decreases as pressure is increased (indicated by the color of the data point).

imaginary components of the relaxation matrix, and we apply the renormalization approach of Ref. [28] to ensure that the relaxation matrix calculated using Equation 12 obeys detailed balance and the sum rule exactly.

Since the collisional transfer rates $K_{j_i j_i'}$ are determined through fits to measured broadening coefficients, the only remaining free parameter in the MEG model is the empirical scaling factor F. F affects the shape of the calculated spectrum, and its value is determined through fits to the spectra measured for this study. Here, we determine F individually for each spectrum in our test matrix spanning 495-977 K and 2-25 bar. Figure 4 shows the F values determined for each of the 12 spectra in the test matrix. Figure 4 shows that the measured F values are both pressure and temperature dependent. The measured F values monotonically decrease with increasing gas pressure. For example, F decreases from ~0.72 to ~0.55 as pressure is increased from 2 to 25 bar at a temperature of ~495 K. The values do not exhibit a clear relationship with gas density. Several past studies have noted the pressure dependence of the F parameter, which is generally judged to

$\bar{F}_{494\,K}$	$\bar{F}_{732\,K}$	$\bar{F}_{970\,K}$
0.631	0.786	0.834

Table 4: Pressure-averaged F parameters for the MEG model ($\bar{F}$) at the three temperatures shown in Figure 4.

be nonphysical and an indicator of the breakdown on the MEG approach for modeling collisional transfer rates [54–56]. As such, we assume pressure-averaged F values in the MEG model for the remainder of this paper. These values are listed in Table 4.

Figure 4 also shows that F depends strongly on temperature, with the pressure-averaged F value increasing by ~30% as the temperature is increased from ~495 K to ~970 K. We can interpret this temperature dependence as a consequence of the approximate nature of the MEG model. Since the MEG model is only an approximate model for the collisional transfer rates, its scaling with temperature is also approximate. As such, the observed temperature-dependence of the F parameter is likely compensating for the imperfect scaling of the MEG model with temperature. To the best of our knowledge, this is the first study to report the temperature dependence of the F parameter for the MEG model.

It is also useful to compare spectra calculated with the MEG model to measured spectra and the spectra calculated with the ECS model. Figure 5 shows this comparison for two spectra measured at 493 K and 25.0 bar, and 964 K and 14.9 bar. The comparison shows that the MEG model calculations (assuming pressure-averaged F values) agree well with the measured spectra, and significantly improve agreement relative to the calculations neglecting line mixing effects. The agreement between the MEG and ECS model calculations is comparable, with RMS deviations from the spectrum measured at 964 K and 14.9 bar being 0.004 and 0.005 for the MEG and ECS calculations, respectively. These results indicate that the MEG model is an effective method to model spectra measured at high pressures and temperatures despite being approximate in nature. However, it is important to note that the level of agreement shown in Figure 5 is only obtained by accurately determining the F scaling factor and its temperature dependence, which is purely empirical in nature. It is also unclear how the F parameters depend on the gas composition (i.e. pure CO_2 or mixtures), or whether the values determined for this wavenumber range will

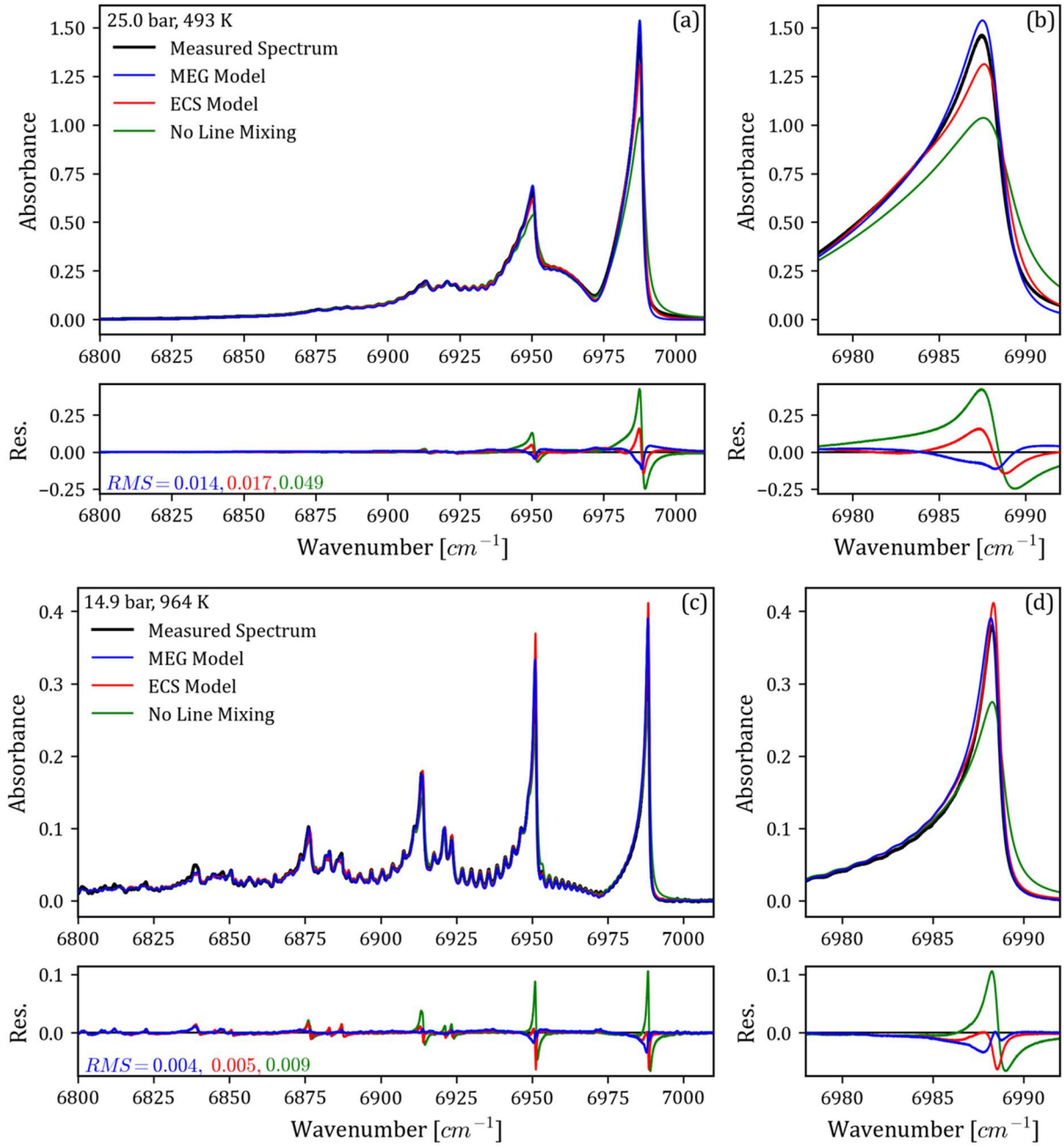

Figure 5: Comparison of measured spectra to spectra calculated using the MEG model (blue), the updated ECS model (red), and a model neglecting line mixing effects (green). Panels (a) and (b) show a comparison for a spectrum measured at 25.0 bar and 493 K. Panels (c) and (d) show a comparison at 14.9 bar and 964 K. The rightmost panels ((b) and (d)) highlight model agreement at the $3\nu_3$ band head.

permit accurate calculations in other bands. These difficulties can be circumvented through the use of the ECS model, which also accurately models the measured spectra and requires fewer modifications and empirical parameters.

4.3. Line Mixing in Phase Spectra

Through the use of the dual-comb spectrometer, it is also possible to study line mixing in the phase spectrum of the absorbing gas for the first time. We present such measurements here in order to explore whether phase spectra can offer unique benefits for the study of line mixing, and to test the performance of the MEG and ECS models at high-density conditions near room temperature.

Measuring the phase spectrum of the absorbing gas requires that only one frequency comb pass through the absorbing gas before being combined with the other comb (often termed the local oscillator) before the detector. A simplified schematic of this configuration is shown in Figure 6(a). The phase spectrum arises from the differential phase shift between the sample and local oscillator comb teeth that is induced by the perturbation to the index of refraction at frequencies near the molecular resonances of the gas in the sample [63]. In this so-called 'asymmetric' dual-comb approach, both the absorption (amplitude) and phase spectrum of the sample gas can be recovered.

Using this approach, we measured amplitude and phase spectra through the high-pressure gas cell at a temperature of 298 K and pressures of 4.92 ± 0.02, 10.16 ± 0.05, and 24.9 ± 0.1 bar. Most experimental and post-processing procedures are the same as for the 'symmetric' dual-comb approach described in earlier sections, with some notable challenges. First, the asymmetric approach requires each frequency comb to propagate in separate optical fibers before being combined and interfered on a photodetector. Perturbations to the two optical fibers can lead to differential phase noise between the two combs. Slow fluctuations in phase from one dual-comb interferogram to the next are compensated by our coherent averaging approach, which is the same method used for the symmetric dual comb experiments described earlier. High-frequency phase noise manifests as an artificial reduction in the measured absorption signal [64]. While we were careful to eliminate this effect in our measurements (e.g. by securing the two optical fibers along collinear paths), it is not possible to rule out small, phase-noise-induced biases in our measured spectra. Second, to preserve optical power, we did not utilize the separate normalization channel described in Section 2. This led to the need for higher-order polynomials in the baseline normalization process than were used for the symmetric cases (see Appendix for a summary of the baseline correction process). Although we were careful to avoid biases, it is difficult to assess whether the higher-order baseline polynomials coupled to residual model error in the baseline

correction process. We assessed the integrated area of the measured amplitude spectra as an indicator of the accuracy of the spectra measured in the phase-sensitive approach. Our results indicate that the integrated areas of the measured spectra agree to within ~1% of expected values based on the HITRAN2020 database.

Figure 6(b) and (c) show amplitude and phase spectra measured at 296 K and 10 bar. The measured spectra are compared to calculated spectra using the ECS and MEG models described in Sections 4.1 and 4.2. Here, we determine the F parameters (Equation 12) required to implement the MEG model at 296 K using the same approach as described in Section 4.2, where in this case the fit to determine each F parameter is between measured and calculated amplitude spectra. We find the pressure-averaged F value to be 0.353 at 296 K. The phase spectrum $\phi(\nu)$ is calculated using both the MEG and ECS models as the real component of the complex spectral profile $\mathcal{J}(\nu)$ [6]

$$\phi(\nu) = Re\{\mathcal{J}(\nu)\} = Re\left\{\frac{1}{\pi}\frac{\sum_{\ell}\sum_{k}\rho_{\ell}(T)d_{\ell}d_{k}\langle\langle k\left\|[\boldsymbol{\Sigma}-\boldsymbol{L_o}-iN\boldsymbol{W}(T)]^{-1}\right\|\ell\rangle\rangle}{\sum_{\ell}\rho_{\ell}(T)d_{\ell}^{2}}\right\} \tag{13}$$

where the parameters are defined as in Equation 1. The absorption coefficient (Equation 1) is associated with the imaginary component of the complex spectra profile, $Im\{\mathcal{J}(\nu)\}$. We use the spectra measured in both amplitude and phase to evaluate the MEG and ECS models for room temperature conditions.

Figure 6 shows that the ECS model significantly improves agreement with the measured spectra (in both amplitude and phase) when compared to both the MEG model and the calculation neglecting line mixing effects. In this case, the MEG model significantly over predicts absorption in the region between the P- and R-branches as well as at the band head. This behavior is not exhibited in comparisons to the higher temperature spectra (e.g. Figure 5), and suggests that the MEG model is not scaling properly to room temperature conditions where gas density is highest. The ECS model, which is based on a more physically realistic description of line mixing, exhibits significantly better agreement with the measured spectra at the high densities near room temperature.

Figure 6 also presents the opportunity to explore the differences between amplitude and phase measurements for fundamental studies of line mixing. Here, Figure 6 shows that the shape of the residuals are qualitatively similar for the model comparisons in both amplitude and phase,

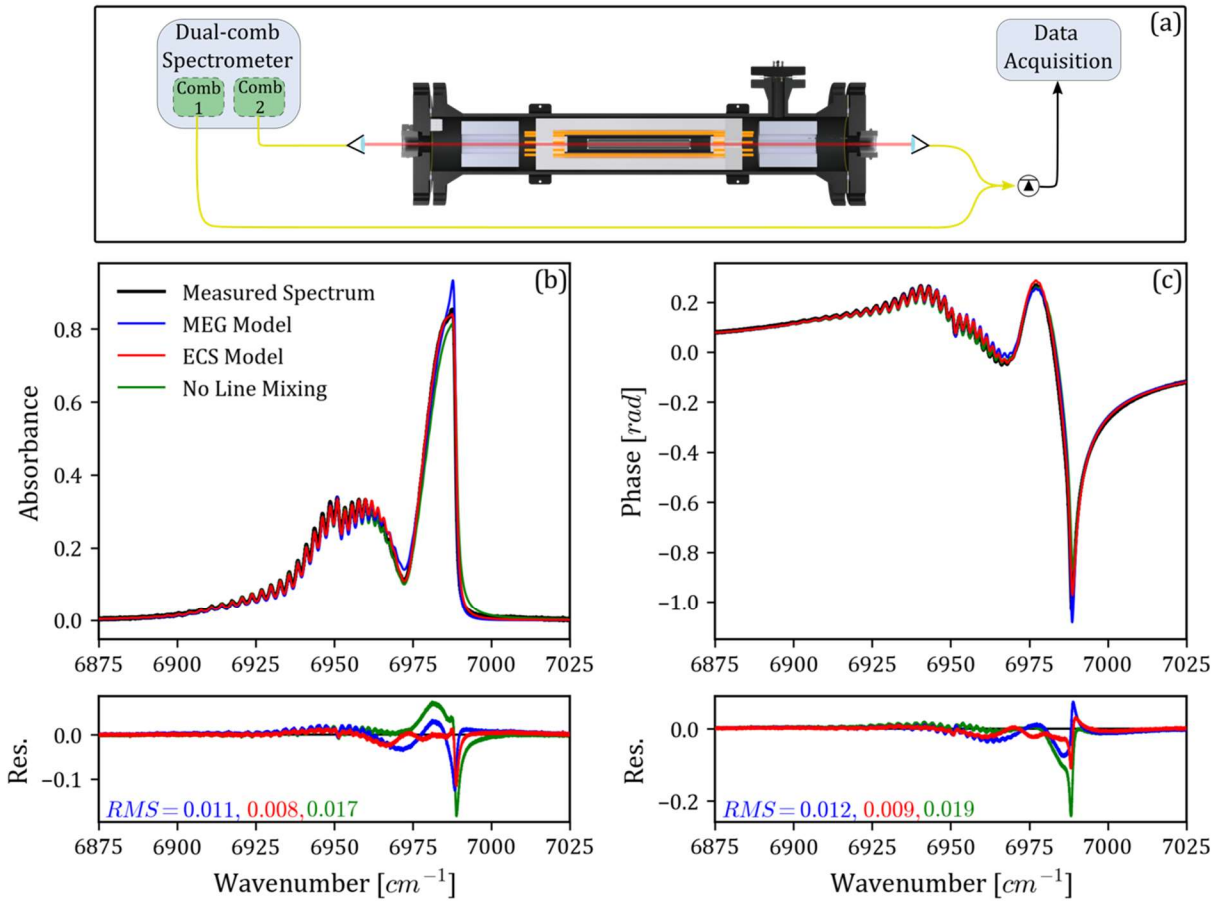

Figure 6: Panel (a) shows a simplified schematic of the 'asymmetric' dual comb approach used to measure amplitude and phase spectra at high pressures near 298 K. Panel (b) shows an absorption (amplitude) spectrum measured at 298 K and 10.16 bar along with spectra calculated using the updated ECS model (red), the MEG model (blue) and a Lorentzian model neglecting line mixing effects (green). Panel (c) shows the same comparison for the measured phase spectrum. In both the absorption and phase spectrum, the updated ECS model demonstrates significantly better agreement with the measurement relative to the MEG and Lorentzian models.

and the RMS of the residuals agree well for the three models across the amplitude and phase measurements. These similarities are expected since the amplitude and phase response can be derived from each other through the Kramers-Kronig relations. Phase measurements may still provide some experimental benefits for future studies of line mixing. For example, although we did not employ a reference path for baseline normalization in these specific measurements, future studies may exploit the fact that phase measurements exhibit reduced baseline fluctuations when compared to amplitude measurements that can be distorted by spectrum-to-spectrum fluctuations in the intensity spectrum of the source. Since baseline correction is a significant source of error

when measuring reference spectra at high pressures, phase measurements may ultimately provide a pathway to eliminate a significant uncertainty source when measuring reference spectra for future studies of line mixing.

5. Summary and Conclusion

We present a systematic study of line mixing and its temperature dependence in the CO_2 bands between 6800 and 7000 cm^{-1}. Our results are based on measurements of pure CO_2 spectra recorded with a broadband, high-resolution (0.0066 cm^{-1}) dual frequency comb absorption spectrometer in a specialized, high-pressure, high-temperature gas cell at conditions up to 977 K and 25 bar. We use our unique measurements to test and improve the pure CO_2 ECS line mixing model of Tran *et al.* for high-temperature spectra up to 977 K. We provide a new set of ECS model parameters validated up to 977 K, and report the temperature dependence of the new parameters required to scale the model over wide temperature ranges. We show that the new, temperature-dependent parameter set significantly improves agreement between measured and calculated spectra for pressures up to 25 bar and over a wide range of temperatures spanning 298-977 K.

We also develop a simpler line mixing model using the modified exponential gap (MEG) scaling law, and we report new measurements of the MEG model parameters and their temperature-dependence. Spectra calculated using the MEG model give good agreement with our measured spectra, however we show that the model depends on a set of pressure- and temperature-dependent scaling parameters (F) that must be accurately determined across the full range of conditions in which the model will be used. Our study is the first to report the temperature dependence of these scaling parameters, which we interpret as being indicative of the approximate nature of the MEG model. Additionally, we show that the accuracy of the MEG model does not scale to spectra measured near room temperature, while the more advanced ECS model permits accurate calculations across the full temperature range of our study (298-977 K).

Finally, we report broadband phase spectra of CO_2 measured at pressures up to 25 bar at room temperature, and present the first comparisons of line mixing models to phase spectra. We compare the phase spectra to spectra calculated using the ECS and MEG models, and discuss how phase spectra could be employed in future studies of line mixing in high pressure gases. These measurements represent the first study of line mixing using phase spectroscopy.

Taken as a whole, our results leverage a unique set of measurements to significantly improve models for line mixing and its temperature dependence in spectra measured at high pressure and temperature. These models can be used in future studies to more accurately calculate spectra at high pressures and temperatures to support applications ranging from optical combustion diagnostics to planetary science.

Acknowledgements

This work is supported by the Air Force Office of Scientific Research (AFOSR) under grant number FA9550-17-1-0224. R. Cole acknowledges support from NASA Headquarters under the NASA Earth and Space Science Fellowship Program (PLANET17F-0120, 18-PLANET18R-0018, 19-PLANET19R-0008).

Appendix

Spectra measured with the dual-comb spectrometer must be corrected for the non-absorbing intensity spectrum of the spectrometer (the 'baseline') before comparing the measured spectra to an absorption model. This baseline correction process can be a significant source of uncertainty when measuring spectra at high pressures and temperatures because the sample gas can absorb continuously over wide frequency ranges. Here, we describe the baseline-correction approach used in the present study and its associated uncertainty.

We normalize our measured spectra using a spectrum measured while the gas cell is held under vacuum and also using a second reference spectrum recorded at the same time as the sample spectrum through an optical path that passes through an identical set of optics as the gas cell (quartz and sapphire windows) but does not pass though the gas cell itself (see Figure 1). The final, normalized transmission spectrum $I(\nu)$ is determined from these spectra as

$$I(\nu) = \left[\frac{I_{cell}}{I_{cell,0}}\right]\left[\frac{I_{ref}}{I_{ref,0}}\right]^{-1} \tag{14}$$

where I_{cell} is the CO_2 transmission spectrum measured through the high-pressure, high-temperature gas cell, I_{ref} is the spectrum measured through the non-absorbing reference cell (see Figure 1), and the subscript "0" refers to spectra measured while the gas cell is held under vacuum. Using this approach, the first term in Equation 14 provides a first-order normalization of the measured spectrum, while the second term provides an additional correction that accounts for

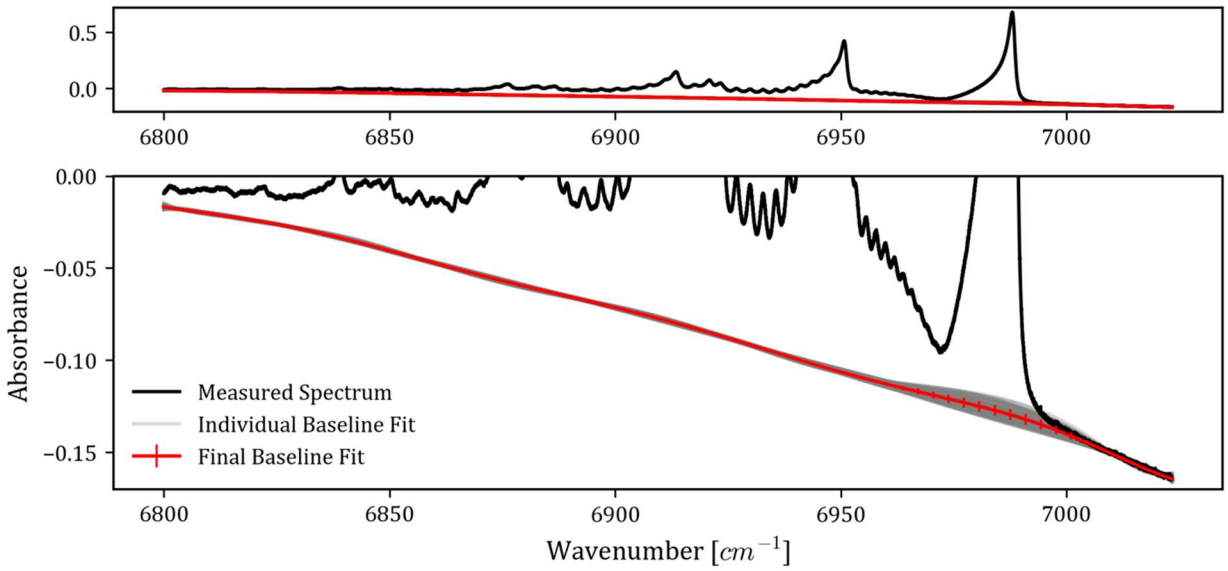

Figure 7: An example baseline-correction result for a spectrum measured at 730 K and 20.0 bar. The top panel shows the full measured spectrum, while the bottom panel highlights the baseline fit. Individual baseline polynomials fit using the randomized process are shown in gray. The final baseline is shown in red, and is determined as the average of the individual fits. Error bars indicate the estimated uncertainty in the final baseline, estimated as the standard deviation of the individual fits.

temporal drift in the native intensity spectrum of the dual-comb spectrometer. In practice, small residual baseline fluctuations remain after this normalization process due to changes in transmission through the gas cell as the system is pressurized. We account for these fluctuations by fitting the normalized spectrum using a single Chebyshev polynomial to account for the remaining baseline contribution. The fitting process uses an absorption model to mask the absorption information while fitting the Chebyshev polynomial. We used spectra calculated using the MEG model (Section 4.2) for this purpose.

One must be careful to avoid introducing user bias in the baseline correction process (i.e. by selecting improper model parameters that couple the measured spectrum with the absorption model used in baseline correction). We addressed this user bias in two ways. First, we masked regions of significant model error (e.g. band heads) in the polynomial fit to avoid allowing excessive model error to influence the baseline-corrected spectrum. Second, we developed a randomized approach to the polynomial fit. For each measured spectrum, we ran the polynomial fit 100 times. In each iteration, we randomly selected the number of polynomial fit coefficients from a pre-defined range of possible values. We then took the final baseline as the average of the individual fits, and used the RMS of the individual polynomials to estimate the uncertainty in the

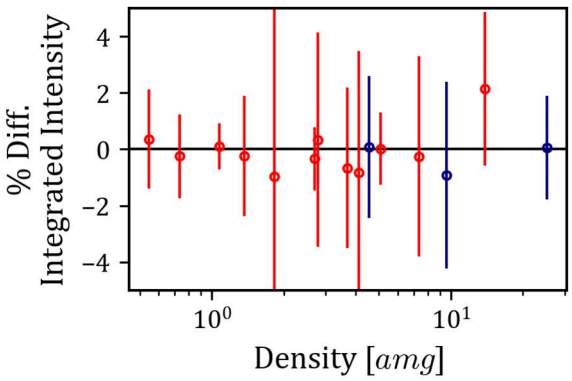

Figure 8: Percent difference between the integrated intensity of the measured, baseline-corrected spectra and the integrated intensity of a HITRAN2020-based model. Spectra measured in the phase-sensitive dual-comb approach (Section 4.3) are shown in blue. Differences remain within 2% for all spectra included in this study.

measured spectrum due to the baseline correction. An example baseline fit utilizing this process is shown in Figure 7.

In practice, we found that the baseline correction approach described above provided a stable means to account for the residual baseline variations without being overly sensitive to absorption model error. For example, repeated runs of the baseline correction code converged on the same baseline fit, and minor adjustments to the absorption model used for baseline correction did not significantly affect the baseline estimate. To test the quality of the baseline-corrected spectra, we compared the integrated intensity of our measured, baseline-corrected spectra to the integrated intensities of spectra simulated using the HITRAN2020 database. This comparison is shown in Figure 8. In this case, baseline errors (or other experimental errors) would manifest as differences between the measured and predicted intensities. Figure 8 shows that the measured intensities agree with the HITRAN predictions within ~2%.

References

1. J. J. Fortney, T. D. Robinson, S. Domagal-Goldman, D. S. Amundsen, M. Brogi, M. Claire, D. Crisp, E. Hebrard, H. Imanaka, R. de Kok, M. S. Marley, D. Teal, T. Barman, P. Bernath, A. Burrows, D. Charbonneau, R. S. Freedman, D. Gelino, C. Helling, K. Heng, A.

G. Jensen, S. Kane, E. M.-R. Kempton, R. K. Kopparapu, N. K. Lewis, M. Lopez-Morales, J. Lyons, W. Lyra, V. Meadows, J. Moses, R. Pierrehumbert, O. Venot, S. X. Wang, and J. T. Wright, "The Need for Laboratory Work to Aid in The Understanding of Exoplanetary Atmospheres," arXiv:1602.06305 [astro-ph] (2016).

2. C. S. Goldenstein, R. M. Spearrin, Jay. B. Jeffries, and R. K. Hanson, "Infrared laser-absorption sensing for combustion gases," Progress in Energy and Combustion Science **60**, 132–176 (2017).

3. P. Niraula, J. de Wit, I. E. Gordon, R. J. Hargreaves, C. Sousa-Silva, and R. V. Kochanov, "The impending opacity challenge in exoplanet atmospheric characterization," Nat Astron 1–9 (2022).

4. Y. Tan, F. M. Skinner, S. Samuels, R. J. Hargreaves, R. Hashemi, and I. E. Gordon, "H_2, He, and CO_2 Pressure-induced Parameters for the HITRAN Database. II. Line Lists of CO_2, N_2O, CO, SO_2, OH, OCS, H_2CO, HCN, PH_3, H_2S, and GeH_4," ApJS **262**(2), 40 (2022).

5. A. T. Basilevsky and J. W. Head, "The surface of Venus," Rep. Prog. Phys. **66**(10), 1699–1734 (2003).

6. J.-M. Hartmann, C. Boulet, and D. Robert, *Collisional Effects on Molecular Spectra: Laboratory Experiments and Models, Consequences for Applications*, 1. ed (Elsevier, 2008).

7. A. Lévy, N. Lacome, and C. Chackerian Jr., "Collisional Line Mixing," in *Spectroscopy of the Earth's Atmosphere and Interstellar Medium*, K. N. Rao and A. Weber, eds. (Academic Press, 1992), pp. 261–337.

8. J.-M. Hartmann, H. Tran, R. Armante, C. Boulet, A. Campargue, F. Forget, L. Gianfrani, I. Gordon, S. Guerlet, M. Gustafsson, J. T. Hodges, S. Kassi, D. Lisak, F. Thibault, and G. C. Toon, "Recent advances in collisional effects on spectra of molecular gases and their practical consequences," Journal of Quantitative Spectroscopy and Radiative Transfer (2018).

9. N. N. Filippov, R. E. Asfin, T. N. Sinyakova, I. M. Grigoriev, T. M. Petrova, A. M. Solodov, A. A. Solodov, and J. V. Buldyreva, "Experimental and theoretical studies of CO_2 spectra for planetary atmosphere modelling: region 600–9650 cm^{-1} and pressures up to 60 atm," Physical Chemistry Chemical Physics **15**(33), 13826–13834 (2013).

10. J. Hartmann and C. Boulet, "Line mixing and finite duration of collision effects in pure CO_2 infrared spectra: Fitting and scaling analysis," The Journal of Chemical Physics **94**(10), 6406–6419 (1991).

11. H. Tran, C. Boulet, S. Stefani, M. Snels, and G. Piccioni, "Measurements and modelling of high pressure pure CO_2 spectra from 750 to 8500 cm_{-1}. I—central and wing regions of the allowed vibrational bands," Journal of Quantitative Spectroscopy and Radiative Transfer **112**(6), 925–936 (2011).

12. N. N. Filippov, J.-P. Bouanich, J.-M. Hartmann, L. Ozanne, C. Boulet, M. V. Tonkov, F. Thibault, and R. Le Doucen, "Line-mixing effects in the $3v_3$ band of CO_2 perturbed by Ar," Journal of Quantitative Spectroscopy and Radiative Transfer **55**(3), 307–320 (1996).

13. F. Thibault, J. Boissoles, R. L. Doucen, V. Menoux, and C. Boulet, "Line mixing effects in the 00°3–00°0 band of CO_2 in helium. I. Experiment," J. Chem. Phys. **100**(1), 210–214 (1994).

14. L. Ozanne, Q. Ma, Nguyen-Van-Thanh, C. Brodbeck, J. P. Bouanich, J. M. Hartmann, C. Boulet, and R. H. Tipping, "Line-mixing, finite duration of collision, vibrational shift, and non-linear density effects in the ν_3 and $3\nu_3$ bands of CO_2 perturbed by Ar up to 1000 bar," Journal of Quantitative Spectroscopy and Radiative Transfer **58**(2), 261–277 (1997).

15. J. M. Hartmann and F. L'Haridon, "Simple modeling of line-mixing effects in IR bands. I. Linear molecules: Application to CO_2," J. Chem. Phys. **103**(15), 6467–6478 (1995).

16. C. Cousin, R. Le Doucen, C. Boulet, A. Henry, and D. Robert, "Line coupling in the temperature and frequency dependences of absorption in the microwindows of the 4.3 μm CO_2 band," Journal of Quantitative Spectroscopy and Radiative Transfer **36**(6), 521–538 (1986).

17. J. Lamouroux, J.-M. Hartmann, H. Tran, B. Lavorel, M. Snels, S. Stefani, and G. Piccioni, "Molecular dynamics simulations for CO_2 spectra. IV. Collisional line-mixing in infrared and Raman bands," J. Chem. Phys. **138**(24), 244310 (2013).

18. J. Lamouroux, L. Régalia, X. Thomas, J. Vander Auwera, R. R. Gamache, and J.-M. Hartmann, "CO_2 line-mixing database and software update and its tests in the 2.1μm and 4.3μm regions," Journal of Quantitative Spectroscopy and Radiative Transfer **151**, 88–96 (2015).

19. D. D. Lee, F. A. Bendana, A. P. Nair, D. I. Pineda, and R. M. Spearrin, "Line mixing and broadening of carbon dioxide by argon in the ν_3 bandhead near 4.2 μm at high temperatures and high pressures," Journal of Quantitative Spectroscopy and Radiative Transfer **253**, 107135 (2020).

20. J. Boissoles, V. Menoux, R. Le Doucen, C. Boulet, and D. Robert, "Collisionally induced population transfer effect in infrared absorption spectra. II. The wing of the Ar-broadened ν_3 band of CO_2," J. Chem. Phys. **91**(4), 2163–2171 (1989).

21. F. Thibault, J. Boissoles, C. Boulet, L. Ozanne, J. P. Bouanich, C. F. Roche, and J. M. Hutson, "Energy corrected sudden calculations of linewidths and line shapes based on coupled states cross sections: The test case of CO_2–argon," J. Chem. Phys. **109**(15), 6338–6345 (1998).

22. J. Boissoles, R. Le Doucen, F. Thibault, and C. Boulet, "The $3\nu_3$ band of CO_2—influence of the pressurized perturber gas," Journal of Quantitative Spectroscopy and Radiative Transfer **52**(3), 361–366 (1994).

23. B. Khalil, O. Cisse, G. Moreau, F. Thibault, R. Le Doucen, and J. Boissoles, "Line mixing and line broadening in CO_2 bands perturbed by helium at 193 K," Chemical Physics Letters **263**(6), 811–816 (1996).

24. A. Predoi-Cross, A. D. May, A. Vitcu, J. R. Drummond, J.-M. Hartmann, and C. Boulet, "Broadening and line mixing in the $20\,0\,0 \leftarrow 01\,1\,0$, $11\,1\,0 \leftarrow 00\,0\,0$ and $12\,2\,0 \leftarrow 01\,1\,0$ Q branches of carbon dioxide: Experimental results and energy-corrected sudden modeling," The Journal of Chemical Physics **120**(22), 10520–10529 (2004).

25. J. Boissoles, F. Thibault, R. L. Doucen, V. Menoux, and C. Boulet, "Line mixing effects in the 00°3–00°0 band of CO_2 in helium. II. Theoretical analysis," J. Chem. Phys. **100**(1), 215–223 (1994).

26. J. Boissoles, F. Thibault, R. Le Doucen, V. Menoux, and C. Boulet, "Line mixing effects in the 0003–0000 band of CO_2 in helium. III. Energy corrected sudden simultaneous fit of linewidths and near wing profile," J. Chem. Phys. **101**(8), 6552–6558 (1994).

27. A. E. DePristo, S. D. Augustin, R. Ramaswamy, and H. Rabitz, "Quantum number and energy scaling for nonreactive collisions," J. Chem. Phys. **71**(2), 850–865 (1979).

28. F. Niro, C. Boulet, and J.-M. Hartmann, "Spectra calculations in central and wing regions of CO_2 IR bands between 10 and 20μm. I: model and laboratory measurements," Journal of Quantitative Spectroscopy and Radiative Transfer **88**(4), 483–498 (2004).

29. R. Rodrigues, K. W. Jucks, N. Lacome, Gh. Blanquet, J. Walrand, W. A. Traub, B. Khalil, R. Le doucen, A. Valentin, C. Camy-peyret, L. Bonamy, and J.-M. Hartmann, "Model, Software, and Database for Computation of Line-Mixing Effects in Infrared Q Branches of Atmospheric CO2—I. Symmetric Isotopomers," Journal of Quantitative Spectroscopy and Radiative Transfer **61**(2), 153–184 (1999).

30. J. Li, A. P. Nair, K. K. Schwarm, D. I. Pineda, and R. Mitchell Spearrin, "Temperature-dependent line mixing in the R-branch of the ν_3 band of methane," Journal of Quantitative Spectroscopy and Radiative Transfer **255**, 107271 (2020).

31. B. Lavorel, G. Millot, J. Bonamy, and D. Robert, "Study of rotational relaxation fitting laws from calculations of SRS N_2 Q-branch," Chemical Physics **115**(1), 69–78 (1987).

32. B. Lavorel, G. Millot, R. Saint-Loup, H. Berger, L. Bonamy, J. Bonamy, and D. Robert, "Study of collisional effects on band shapes of the $\nu_1/2\nu_2$ Fermi dyad in CO_2 gas with stimulated Raman spectroscopy. I. Rotational and vibrational relaxation in the 2ν2 band," J. Chem. Phys. **93**(4), 2176–2184 (1990).

33. C. A. Almodovar, W.-W. Su, R. Choudhary, J. Shao, C. L. Strand, and R. K. Hanson, "Line mixing in the nitric oxide R-branch near 5.2 μm at high pressures and temperatures: Measurements and empirical modeling using energy gap fitting," Journal of Quantitative Spectroscopy and Radiative Transfer **276**, 107935 (2021).

34. F. A. Bendana, D. D. Lee, C. Wei, D. I. Pineda, and R. M. Spearrin, "Line mixing and broadening in the ν(1→3) first overtone bandhead of carbon monoxide at high temperatures and high pressures," Journal of Quantitative Spectroscopy and Radiative Transfer **239**, 106636 (2019).

35. D. D. Lee, F. A. Bendana, A. P. Nair, S. A. Danczyk, W. A. Hargus, and R. M. Spearrin, "Exploiting line-mixing effects for laser absorption spectroscopy at extreme combustion pressures," Proceedings of the Combustion Institute **38**(1), 1685–1693 (2021).

36. M. Gu, S. Wang, G. Wang, Q. Wang, X. Liu, F. Qi, and C. S. Goldenstein, "Improved laser absorption spectroscopy measurements of flame temperature via a collisional line-mixing model for CO2 spectra near 4.17 μm," Appl. Phys. B **128**(7), 131 (2022).

37. R. K. Cole, A. D. Draper, P. J. Schroeder, C. M. Casby, A. S. Makowiecki, S. C. Coburn, J. E. Steinbrenner, N. Hoghooghi, and G. B. Rieker, "Demonstration of a uniform, high-

pressure, high-temperature gas cell with a dual frequency comb absorption spectrometer," Journal of Quantitative Spectroscopy and Radiative Transfer **268**, 107640 (2021).

38. I. Coddington, N. Newbury, and W. Swann, "Dual-comb spectroscopy," Optica **3**(4), 414 (2016).
39. G.-W. Truong, E. M. Waxman, K. C. Cossel, E. Baumann, A. Klose, F. R. Giorgetta, W. C. Swann, N. R. Newbury, and I. Coddington, "Accurate frequency referencing for fieldable dual-comb spectroscopy," Opt. Express **24**(26), 30495–30504 (2016).
40. S. Coburn, C. B. Alden, R. Wright, K. Cossel, E. Baumann, G.-W. Truong, F. Giorgetta, C. Sweeney, N. R. Newbury, K. Prasad, I. Coddington, and G. B. Rieker, "Regional trace-gas source attribution using a field-deployed dual frequency comb spectrometer," Optica **5**(4), 320–327 (2018).
41. P. J. Schroeder, R. J. Wright, S. Coburn, B. Sodergren, K. C. Cossel, S. Droste, G. W. Truong, E. Baumann, F. R. Giorgetta, I. Coddington, N. R. Newbury, and G. B. Rieker, "Dual frequency comb laser absorption spectroscopy in a 16 MW gas turbine exhaust," Proceedings of the Combustion Institute **36**(3), 4565–4573 (2016).
42. A. D. Draper, R. K. Cole, A. S. Makowiecki, J. Mohr, A. Zdanowicz, A. Marchese, N. Hoghooghi, and G. B. Rieker, "Broadband dual-frequency comb spectroscopy in a rapid compression machine," Optics Express **27**(8), 10814 (2019).
43. E. W. Lemmon, M. L. Huber, and M. O. McLinden, "NIST REFPROP: Reference Fluid Thermodynamic and Transport Properties," (2007).
44. R. Span and W. Wagner, "A New Equation of State for Carbon Dioxide Covering the Fluid Region from the Triple-Point Temperature to 1100 K at Pressures up to 800 MPa," Journal of Physical and Chemical Reference Data **25**(6), 1509–1596 (1996).
45. I. Coddington, W. C. Swann, and N. R. Newbury, "Coherent dual-comb spectroscopy at high signal-to-noise ratio," Physical Review A **82**(4), 043817 (2010).
46. I. E. Gordon, L. S. Rothman, R. J. Hargreaves, R. Hashemi, E. V. Karlovets, F. M. Skinner, E. K. Conway, C. Hill, R. V. Kochanov, Y. Tan, P. Wcisło, A. A. Finenko, K. Nelson, P. F. Bernath, M. Birk, V. Boudon, A. Campargue, K. V. Chance, A. Coustenis, B. J. Drouin, J. –M. Flaud, R. R. Gamache, J. T. Hodges, D. Jacquemart, E. J. Mlawer, A. V. Nikitin, V. I. Perevalov, M. Rotger, J. Tennyson, G. C. Toon, H. Tran, V. G. Tyuterev, E. M. Adkins, A. Baker, A. Barbe, E. Canè, A. G. Császár, A. Dudaryonok, O. Egorov, A. J. Fleisher, H. Fleurbaey, A. Foltynowicz, T. Furtenbacher, J. J. Harrison, J. –M. Hartmann, V. –M. Horneman, X. Huang, T. Karman, J. Karns, S. Kassi, I. Kleiner, V. Kofman, F. Kwabia–Tchana, N. N. Lavrentieva, T. J. Lee, D. A. Long, A. A. Lukashevskaya, O. M. Lyulin, V. Yu. Makhnev, W. Matt, S. T. Massie, M. Melosso, S. N. Mikhailenko, D. Mondelain, H. S. P. Müller, O. V. Naumenko, A. Perrin, O. L. Polyansky, E. Raddaoui, P. L. Raston, Z. D. Reed, M. Rey, C. Richard, R. Tóbiás, I. Sadiek, D. W. Schwenke, E. Starikova, K. Sung, F. Tamassia, S. A. Tashkun, J. V. Auwera, I. A. Vasilenko, A. A. Vigasin, G. L. Villanueva, B. Vispoel, G. Wagner, A. Yachmenev, and S. N. Yurchenko, "The HITRAN2020 molecular spectroscopic database," Journal of Quantitative Spectroscopy and Radiative Transfer 107949 (2021).

47. J. Yang, P. J. Schroeder, M. J. Cich, F. R. Giorgetta, W. C. Swann, I. Coddington, N. R. Newbury, B. J. Drouin, and G. B. Rieker, "Speed-dependent Voigt lineshape parameter database from dual frequency comb measurements at temperatures up to 1305 K. Part II: Argon-broadened H_2O absorption, 6801–7188 cm^{-1}," Journal of Quantitative Spectroscopy and Radiative Transfer **217**, 189–212 (2018).

48. R. Rodrigues, C. Boulet, L. Bonamy, and J. M. Hartmann, "Temperature, pressure, and perturber dependencies of line-mixing effects in CO_2 infrared spectra. II. Rotational angular momentum relaxation and spectral shift in Σ←Σ bands," J. Chem. Phys. **109**(8), 3037–3047 (1998).

49. A. R. Edmonds, *Angular Momentum in Quantum Mechanics*, Princeton Landmarks in Physics (Princeton University Press, 1996).

50. F. Rachet, M. Margottin-Maclou, A. Henry, and A. Valentin, "Q-Branch Line Mixing Effects in the (2000)I← 0110 and (1220)I← 0110 Bands of Carbon Dioxide Perturbed by N_2, O_2, and Ar and in the 1310 ← 0000 and 1310 ← 0110 Bands of Pure Nitrous Oxide," Journal of Molecular Spectroscopy **175**(2), 315–326 (1996).

51. J. I. Steinfeld, P. Ruttenberg, G. Millot, G. Fanjoux, and B. Lavorel, "Scaling laws for inelastic collision processes in diatomic molecules," J. Phys. Chem. **95**(24), 9638–9647 (1991).

52. R. K. Cole, N. Hoghooghi, B. J. Drouin, and G. B. Rieker, "High-temperature absorption line shape parameters for CO_2 in the 6800–7000 cm^{-1} region from dual frequency comb measurements up to 1000 K," Journal of Quantitative Spectroscopy and Radiative Transfer **276**, 107912 (2021).

53. C. J. Meinrenken, W. D. Gillespie, S. Macheret, W. R. Lempert, and R. B. Miles, "Time domain modeling of spectral collapse in high density molecular gases," J. Chem. Phys. **106**(20), 8299–8309 (1997).

54. A. S. Pine and J. P. Looney, "Self-broadening and line mixing in HCN Q branches," J. Chem. Phys. **96**(3), 1704–1714 (1992).

55. A. S. Pine, "Self-, N_2- and Ar-broadening and line mixing in HCN and C_2H_2," Journal of Quantitative Spectroscopy and Radiative Transfer **50**(2), 149–166 (1993).

56. D. Romanini and K. K. Lehmann, "Line-mixing in the 106←000 overtone transition of HCN," J. Chem. Phys. **105**(1), 81–88 (1996).

57. D. Pieroni, -Van-Thanh Nguyen, C. Brodbeck, C. Claveau, A. Valentin, J. M. Hartmann, T. Gabard, J.-P. Champion, D. Bermejo, and J.-L. Domenech, "Experimental and theoretical study of line mixing in methane spectra. I. The N_2-broadened ν_3 band at room temperature," J. Chem. Phys. **110**(16), 7717–7732 (1999).

58. A. S. Pine and J. P. Looney, "Decoupling in the line mixing of acetylene infrared Q branches," J. Chem. Phys. **93**(10), 6942–6953 (1990).

59. R. G. Gordon, "Semiclassical Theory of Spectra and Relaxation in Molecular Gases," J. Chem. Phys. **45**(5), 1649–1655 (1966).

60. J. Boissoles, C. Boulet, D. Robert, and S. Green, "IOS and ECS line coupling calculation for the CO–He system: Influence on the vibration–rotation band shapes," J. Chem. Phys. **87**(6), 3436–3446 (1987).

61. W. D. Gillespie, C. J. Meinrenken, W. R. Lempert, and R. B. Miles, "Interbranch line-mixing in CO_2 (1001) and (0201) combination bands," J. Chem. Phys. **107**(16), 5995–6004 (1997).

62. M. O. Bulanin, A. B. Dokuchaev, M. V. Tonkov, and N. N. Filippov, "Influence of line interference on the vibration-rotation band shapes," Journal of Quantitative Spectroscopy and Radiative Transfer **31**(6), 521–543 (1984).

63. F. R. Giorgetta, G. B. Rieker, E. Baumann, W. C. Swann, L. C. Sinclair, J. Kofler, I. Coddington, and N. R. Newbury, "Broadband Phase Spectroscopy over Turbulent Air Paths," Phys. Rev. Lett. **115**(10), 103901 (2015).

64. G.-W. Truong, K. C. Cossel, E. M. Waxman, F. R. Giorgetta, I. Coddington, and N. R. Newbury, "Phase Noise-Induced Biases in Coherent Dual-Comb Spectroscopy," in *Conference on Lasers and Electro-Optics (2016), Paper SW1H.2* (Optical Society of America, 2016), p. SW1H.2.